

Microstructure, mechanical, and in vitro properties of mica glass-ceramics with varying fluorine content

Atiar Rahaman Molla · Bikramjit Basu

Received: 10 September 2008 / Accepted: 3 November 2008 / Published online: 26 November 2008
© Springer Science+Business Media, LLC 2008

Abstract The design and development of glass ceramic materials provide us the unique opportunity to study the microstructure development with changes in either base glass composition or heat treatment conditions as well as to understand processing-microstructure-property (mechanical/biological) relationship. In the present work, it is demonstrated how various crystal morphology can develop when F^- content in base glass ($K_2O-B_2O_3-Al_2O_3-SiO_2-MgO-F$) is varied in the range of 1.08–3.85% and when all are heat treated at varying temperatures of 1000–1120°C. For some selected heat treatment temperature, the heat treatment time is also varied over 4–24 h. It was established that with increase in fluoride content in the glass composition, the crystal volume fraction of the glass-ceramic decreases. Using 1.08% fluoride, more than 80% crystal volume fraction could be achieved in the $K_2O-B_2O_3-Al_2O_3-SiO_2-MgO-F$ system. It was observed that with lower fluoride content glass-ceramic, if heated at 1040°C for 12 h, an oriented microstructure with ‘envelop like’ crystals can develop. For glass ceramics with higher fluorine content (2.83% or 3.85%), hexagonal-shaped crystals are formed. Importantly, high hardness of around 8 GPa has been measured in glass ceramics with maximum amount of crystals. The three-point flexural strength and elastic modulus of the glass-ceramic (heat treated at 1040°C for 24 h) was 80 MPa and 69 GPa of the sample

containing 3.85% fluorine, whereas, similar properties obtained for the sample containing 1.08% F^- was 94 MPa and 57 GPa, respectively. Further, in vitro dissolution study of the all three glass-ceramic composition in artificial saliva (AS) revealed that leached fluoride ion concentration was 0.44 ppm, when the samples were immersed in AS for 8 weeks. This was much lower than the WHO recommended safety limits of 1.5 ppm. Among all the investigated glass-ceramic samples, the glass ceramic with 3.85% F^- content in base glass (heat treated at 1040°C for 12 h), exhibits the adherence of Ca–P layer, which consists of spherical particles of 2–3 μm . Other ions, such as Mg^{+2} and K^{+1} ion concentrations in the solution were found to be 8 and 315 ppm after 8 weeks of leaching, respectively. The leaching of all metal ions is recorded to decrease with time, probably due to time-dependent kinetic modification of sample surface. Summarizing, the present study illustrates that it is possible to obtain a good combination of crystallization, mechanical and in vitro dissolution properties with the careful selection of base glass composition and heat treatment conditions.

1 Introduction

Glass-ceramics (GC) with the characteristic microstructure of sheet silicates in the fluorine mica family can be made machinable, strong, thermal shock resistant and with excellent dielectric properties [1]. Glass-ceramics, demonstrating such favorable properties, can be developed with a variety of microstructures by carefully varying the base glass composition and heat treatment conditions [2]. An important group of these materials, i.e., mica containing glass ceramics received wider application due to their high

A. R. Molla
Glass Division, Central Glass and Ceramic Research Institute,
Council of Scientific and Industrial Research (CSIR),
Kolkata 700 032, India

A. R. Molla · B. Basu (✉)
Department of Materials and Metallurgical Engineering,
Indian Institute of Technology Kanpur, Kanpur 208016, India
e-mail: bikram@iitk.ac.in

machinability, which results in an increased versatility of the finished shape. The machinability, as well as other properties, such as high thermal shock resistance and excellent electrical insulation, etc., is attributed to the unique microstructure of an interlocking array of plate-like mica crystals, dispersed throughout a glassy matrix [3, 4]. Also, machinable glass ceramics are potential materials for dental restorations due to possibility of achieving a combination of high machinability, matching mechanical properties with natural teeth, bioactivity and finally, good aesthetics [5–8]. In the development of bioactive materials, Bioglass [9, 10], Ceravita [11], Apatite–Wollastonite (AW) glass-ceramic [12, 13] and dense hydroxyapatite ceramic [14, 15] have been well characterized for clinical applications. These materials either have a close chemical resemblance to bone mineral, or they provide an intimate contact with the surrounding tissue. However, owing to their brittle nature, their applications are limited to cases, where the mechanical stresses, particularly the tensile stress, are nonexistent or sufficiently low. Therefore, a better combination of high strength, hardness, appropriate E-modulus and good in vitro biocompatibility property is an essential requirement for biomaterial; not only because they ensure reliability and long lifetime, but also because they are the indispensable factors that govern the performance and osteoconduction [16] between the implant and living tissue, when used under load-bearing conditions in vivo. Among the bioactive materials mentioned above, A–W glass-ceramic has been reported to have the best mechanical properties and also shows excellent bioactivity in prosthetic applications [17–19]. Quinn et al. [20] reported the influence of microstructure and chemistry on the fracture toughness of various ceramics. However, all the materials mentioned above are not machinable and they do not have a good combination of mechanical properties. To this end, it is easier to process mica-based GC with good mechanical properties into surgical parts with various complex shapes by using normal clinical machining methods [21].

Like other GC, the properties of machinable GC depend on the type, sizes and volume fraction of the primary crystalline phases [22]. Also, the microstructures as well as properties are sensitive towards base glass composition (e.g., fluorine content). The presence of fluorine in the base glass enhances phase separation, and phase separation usually precedes the crystallization. In the glass system of the MAS type (MAS: $\text{MgOAl}_2\text{O}_3\text{SiO}_2$), fluorine has the role of a nucleating agent [23]. Radonjić and his co-workers [23] demonstrated that when fluorine content in glass is high, nucleation starts at relatively lower temperature. Cheng et al. [24] also reported that fluorine source has an effect on the crystallization behavior of the glass ceramics (GC) system. They established that with the NaF

as the source of fluorine, only surface crystallization occurs. In contrast, with MgF_2 as the source of fluorine, uniform bulk crystals can form.

Apart from crystallisation/microstructure development aspect, the in vitro dissolution/leaching of glass ceramics also depends on glass composition or crystal morphology. The present study is a part of our ongoing research in the area of glass ceramics. In our recent work [6, 7], the development of some unusual spherulitic-dendritic crystals as well as their in vitro dissolution properties are reported. One of the sensitive element in $\text{K}_2\text{O}-\text{B}_2\text{O}_3-\text{Al}_2\text{O}_3-\text{SiO}_2-\text{MgO}-\text{F}$ glass compositions is fluorine and therefore, this present study investigates the aspects of microstructure development as well as properties when fluorine content in base glass is varied over a narrow range. This paper will demonstrate how small variation in fluorine will influence significantly the crystallization as well as physical/in vitro dissolution properties of the heat treated glass ceramics. Importantly, it will be shown how the apatite rich surface layer can be formed in specific glass ceramic composition after dissolution in AS. The basic mechanisms operating in dissolution of the material in the solution have been analyzed. It can be noted that the leaching of silicate-based ceramics occurs during exposure to aqueous solutions. In addition, leaching can lead to weakening of the ceramic, roughening of the surface, and increased abrasion potential against contacting surfaces [25]. In summary, the novelty of the present work is to demonstrate the following aspects: (a) how the characteristically different crystal morphologies can be developed with variation in F^- content in the narrow window of 1–4%, (b) how one can develop GC with superior combination of hardness, strength and E-modulus by designing both base glass composition and heat treatment condition, and (c) in vitro dissolution and Ca–P rich layer formation in vitro of the optimized GC.

2 Experimental procedures

2.1 Materials and heat treatment experiments

Three compositions with varying fluorine content in the $\text{K}_2\text{O}-\text{MgO}-\text{Al}_2\text{O}_3-\text{B}_2\text{O}_3-\text{SiO}_2-\text{F}$ have been studied in the present work (Table 1). The starting materials were highly pure optical grade Quartz Flour (Sipur A1 Bremthaler Quarzitwerk, Germany), Aluminum nitrate nona hydrate (Riedel-de-Hahn AG, Germany), Magnesium hydroxide carbonate (Merck, Germany), Potassium nitrate (Merck, Germany), Boric acid (Merck KGaA, Germany), and MgF_2 (Merck KGaA, Germany). Glass batches with desired compositions were mixed using agate and mortar and thereafter, melted in a platinum crucible at 1550°C for 2 h using electrical furnace. The glass melts were cast into a

Table 1 Compositions of base glass (in wt%) used in the present work

Starting materials	Precursor constituent	M1	M2	M3
Quartz powder	SiO ₂	47.98	48.94	42.57
White tabular alumina	Al ₂ O ₃	17.62	16.29	17.81
MgO powder	MgO	19.36	17.45	18.80
K ₂ CO ₃	K ₂ O	8.25	7.15	7.81
Boric acid (H ₃ BO ₃)	B ₂ O ₃	5.17	5.25	10.02
NH ₄ F/MgF ₂	F ⁻	1.08	3.85	2.53

cast iron mould to form plates, and then annealed for 2 h in the temperature range of 600–650°C. The annealing conditions were selected in order to avoid nucleation at this stage. The compositions of the base glasses were analyzed by inductively coupled plasma atomic absorption spectroscopy (ICP-AES, spectroflame modula FTM 08, Germany). Differential thermal analyses (DTA) (Netzsch-Gerätebau GmbH, STA 409C) with the heating rate of 10°C/min were performed over the temperature range of 30–1400°C on the powdered samples to investigate the crystallization behavior of the glasses. XRD study for each glass-ceramic was carried out to determine phase assemblage in the heat treated materials. The X-ray diffraction patterns of the samples were recorded in X’pert pro MPD diffractometer (PANalytical, The Netherlands) operating at 45 kV and 40 mA using Ni-filtered CuK α radiation. The amorphous nature of as-prepared glasses was confirmed by XRD. Two-stage heat-treatment has been done to crystallize the glass and to convert it into glass ceramics. Nucleation was done in the temperature range of 750–850°C. The crystallization experiments were conducted in the temperature range of 1000–1120°C, employing varying time of holding from 4 to 24 h.

2.2 Microstructure and mechanical property characterization

The glass ceramics produced were polished using diamond paste and the polished surface is etched with 12% hydrofluoric acid (HF) with varying time from 1 to 3 min at different zones of the sample for revealing the crystal morphology in the bulk glass ceramic sample. The crystalline phases, precipitated in the glass after crystallization, was also identified by XRD, using powdered sample and observed by SEM-EDS (LEOs 430i, UK). FT-IR (Perkin Elmer, Model 1615) study was done in order to identify different bonds present in the GCs and crystals structure.

The hardness property of the glass ceramic samples was measured by taking micro-indentation on the polished surface of the samples. Micro-indentations are taken using

160 microhardness testers (Carl Zeiss Jena, Germany) equipped with a conical Vicker’s indenter at an indent load of 40 g. About ten indents were taken for each sample with identical loading condition. The diagonals of the Vickers indents were carefully measured using SEM and subsequently, the hardness was calculated using the standard equation for the Vickers geometry.

$$H_v = 1.8554 P/d^2 \tag{1}$$

where H_v is the Vickers hardness number (VHN) in kg/mm², P is the normal load in kg, and d is the average diagonal length of the indentation in mm. Elastic modulus and flexural strength were measured using 3-point bending set up on Instron machine. During 3-point flexural tests, the displacement of the bar sample was measured by placing a linear variable displacement transducer (LVDT) adjacent to the tensile surface. From the slope of the linear part of the obtained load–displacement curve, the E-modulus was measured. The flexural properties were evaluated using the span length of 40 mm and crosshead speed 0.5 mm/min at temperature of 25°C and relative humidity of 70%.

2.3 In vitro tests

As part of the in vitro study, M2 samples were immersed in AS (heat treated at 1040°C for 12 h) for five different time periods (1, 2, 3, 6, and 8 weeks). The justification for selection of M2 GC for in vitro tests will be provided in Subsect. 3.3. The composition of AS has been obtained from literature [26, 27] and is provided in Table 2. The solution and the samples were kept in polyethylene bottles and kept in humidity chamber, maintained at human body temperature of 37.4°C and relative humidity of 40%. The weight loss of the investigated glass-ceramic samples was measured after each dissolution test. SEM images and SEM-EDS analysis of the surface of the M2 sample (heat treated at 1040°C for 12 h), immersed in AS for different time periods of 2, 3, 6, and 8 weeks, were taken in order to assess the extent of Ca–P layer formation on the surface. Atomic Absorption spectroscopy (AAS) (Spectra AA,

Table 2 Composition of artificial saliva [26, 27]

Material	Amount (gm) per 1 L of distilled water	Comment
NaCl	0.4	99.9% pure, AR grade
KCl	0.4	99.5% pure, AR grade
CaCl ₂ · 2H ₂ O	0.795	99.5% pure, AR grade
NaH ₂ PO ₄ · 2H ₂ O	0.78	99% pure, AR grade
Na ₂ S · 9H ₂ O	0.005	99.9% pure, AR grade
Urea	1	99.5% pure, AR grade

AR analytical reagent grade

220FS, Varian, Australia) was used in order to detect the concentration of metal ions in the in vitro test solutions. In a different set of experiments, M1, M2 and M3 GC, heat treated, for 12 h at 1040°C, were also immersed in AS for a period of 8 weeks. The change in Mg^{+2} and K^{+} ions in AS was measured by AAS. The leached F^{-} ion concentration in AS solution was analyzed by inductively coupled plasma atomic absorption spectroscopy (ICP-AES, spectroflame modula FTM 08, Germany).

3 Results

3.1 XRD, DTA and FT-IR data

Extensive X-ray diffractions study was carried out to determine phase assemblage in various heat-treated samples of $K_2O-B_2O_3-Al_2O_3-SiO_2-MgO-F$ system. XRD analysis of the temperature variation batches (heat treated for 12 h in temperature range of 1000–1120°C) for the M1 sample revealed predominant presence of fluorophlogopite (FPP) in all the samples. Variation in peak intensity of various crystalline phases was observed with different temperatures during crystallization heat-treatment of sample M1 (Fig. 1). It is interesting to note that intensity of few peaks was increased with temperature, which confirms the progressive dissolution of norbergite phases and

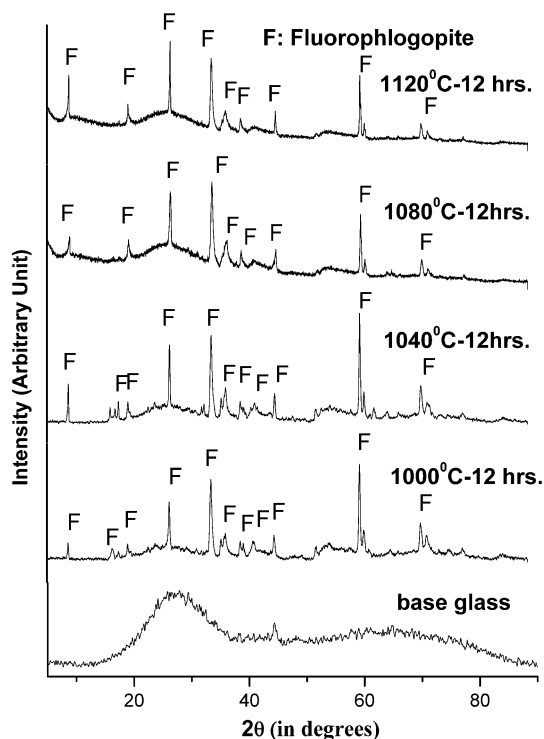


Fig. 1 XRD plot of the heat-treated M1 glass ceramic samples, crystallized at varying temperatures with a constant time of 12 h

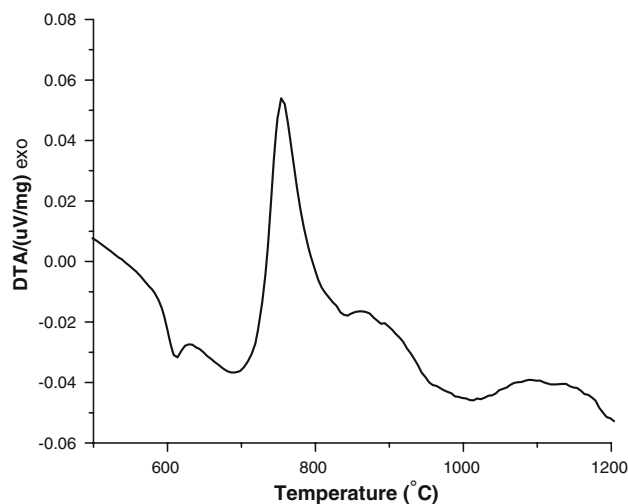


Fig. 2 DTA trace recorded with M1 glass powders

subsequently growth of FPP. Similar results were also obtained for M2 and M3 glass ceramics, heat treated at 1040°C (not shown).

In order to obtain more information on crystallization behavior, DTA analysis of base glass powder was carried out. From the DTA scan of the base glass of M1 composition (Fig. 2), it can be seen that the first crystal phase forms at nearly above 750°C, which is apparent from the large exothermic peak. The glass transition (T_g) temperature is found to be around 603°C, which is evident from the first exothermic peak and subsequent slope change of the curve in the DTA scan. In the DTA diagram, three distinct exothermic peaks are identified at temperatures 754, 843, and 1147°C. These exothermic peaks in the DTA trace are characteristics of chondrotite to norbergite crystal formation (754°C) and evolution of fluorophlogopite (843°C) and its complete dissolution at 1147°C.

Fourier Transform Infrared Spectroscopy (FT-IR) was carried out in order to obtain more structural information on both glass and glass ceramics. FT-IR curves of glass ceramics were compared with the FT-IR of original macor glass ceramics, as reported by Saraswati et al. [28]. Detailed analysis of the FT-IR data confirmed the presence of various Si–O–Si, Si–O and B–O stretching bonds with the characteristic absorption peaks at 1022, 697 and 1422 cm^{-1} , respectively [29]. It has been observed that, there was no major shift in absorption peaks of FT-IR between base glass and glass ceramics. In addition, Si–O–Si bonds cause FT-IR peak as 465–509 cm^{-1} (Fig. 3).

3.2 SEM-EDS analysis of heat-treated glass-ceramics

The detailed SEM analysis was carried out to study crystal shapes, size and size distribution in various heat-treated glass-ceramic samples of varying composition. In the

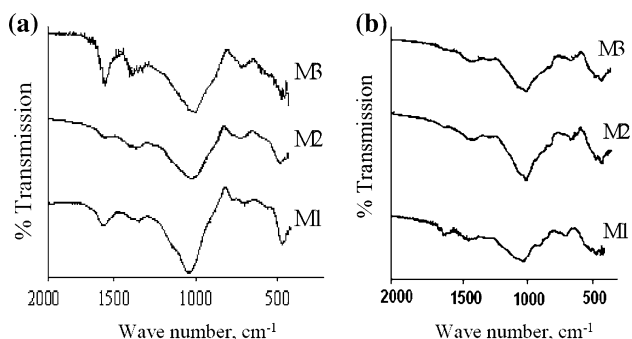


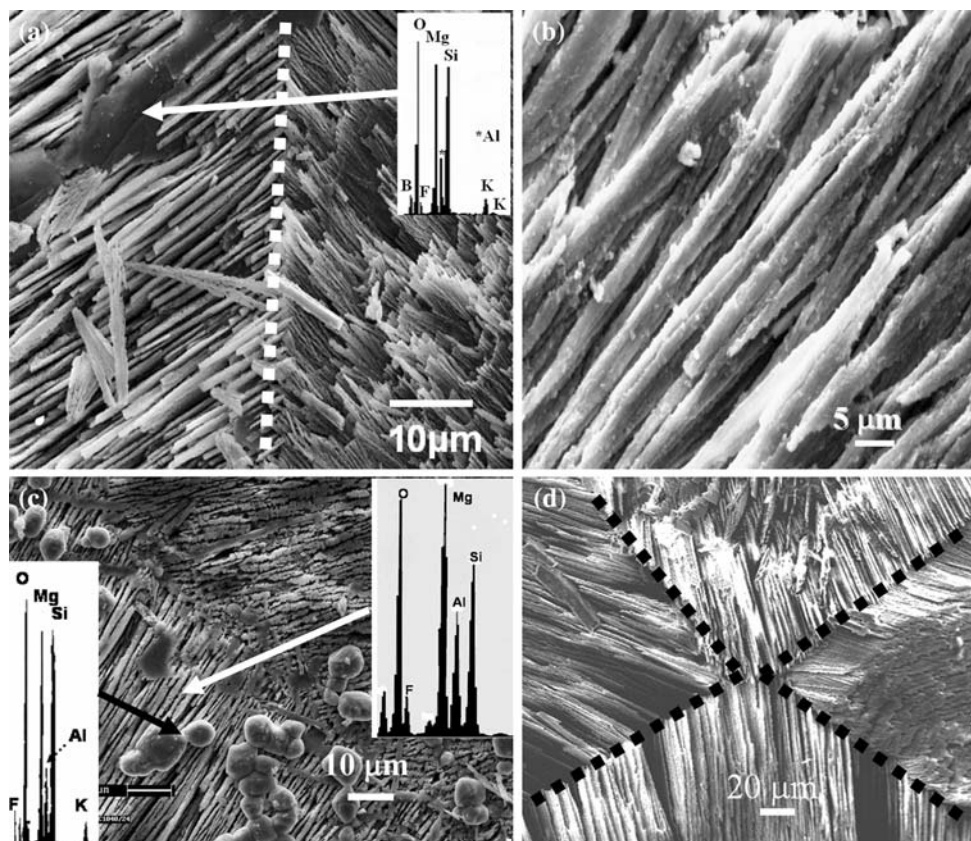
Fig. 3 FT-IR spectra of **a** base glass with samples M1, M2 and M3 composition and **b** glass-ceramics prepared with composition M1, M2 and M3, all heat treated at 1040°C for 12 h

following, some characteristic crystal morphology for some selected samples has been discussed to illustrate the influence of base glass composition and/or heat treatment conditions on crystallization behavior. In Fig. 4, SEM images of M1 glass-ceramic, crystallized at 1040°C for 12 h are provided. The presence of large rod like crystals, aligned in specific directions can be clearly observed in Fig. 4a and b. In Fig. 4a, the presence of residual glass can also be observed. In addition, the boundary between two microstructural regions having rod like crystals, aligned in two different orientations has also been identified by dotted line in Fig. 4a. From Fig. 4b, it is clear that the

characteristic crystals have 3–5 μm in width and also a large aspect ratio. EDS analysis of the residual glass in Fig. 4a indicates strong O-peak, as well as peaks of Si and Mg of equal intensity. In contrast, the EDS analysis of the crystal show Mg-peaks of highest intensity (Fig. 4c), followed by Si and Al (both having equal intensity). Clearly, the relative intensity of O-peak from crystals is much less than that of residual glass. From such observations, it should be clear that the crystals are relatively Mg rich. SEM observation of Fig. 4b reveals that crystals are unidirectionally oriented and glassy droplets are dispersed on crystals. EDS analysis of the glassy phase demonstrates characteristic stronger peaks of oxygen, with Si and Mg peaks of comparable intensity. In Fig. 4d, SEM images of the sample reveal the presence of crystal domain boundary, which are formed by the intersection of crystals growing from different directions. These crystal domain boundaries are distinctly visible in Fig. 4d and the boundary between different crystals is marked with dotted line.

In Fig. 5a, SEM images of M2 glass ceramics, crystallized for 12 h at a temperature of 1120°C is provided. SEM analysis demonstrates crystals with sizes in the range of 5–10 μm. The analysis of EDS spectra of glass (Fig. 5a) reveals similar observations, as earlier described for the M1 samples. In Fig. 5b, SEM image of M3 sample, heat-treated at 1000°C for 9 h is provided. SEM image illustrates

Fig. 4 SEM micrographs of M1 glass ceramics crystallized at 1040°C for 12 h. **a** Oriented mica crystals meeting at a line to form a crystal domain boundary, **b** orientation of individual mica rods of diameter about 2–3 μm, **c** oriented crystals of different morphology meeting at a domain boundary, and **d** highly oriented crystals are meeting at a point forming envelope like crystal morphology. The crystal domain boundaries are identified by the dotted lines in (a) and (d)



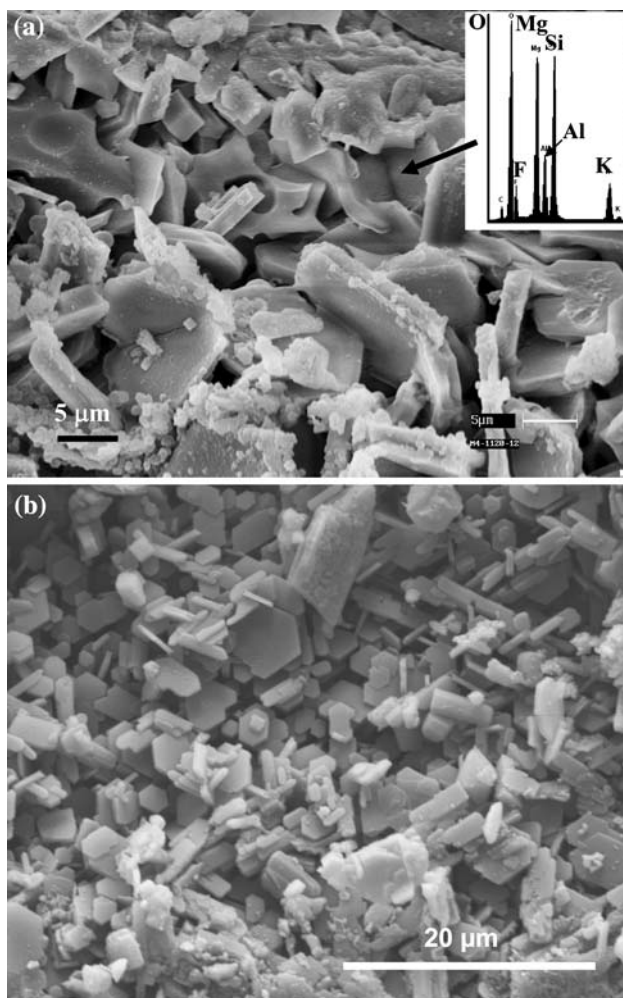


Fig. 5 SEM micrographs of **a** M2 glass-ceramic crystallized for 12 h at a temperature of 1120°C. **b** M3 sample crystallized at 1000°C for 9 h

the presence of dense arrangement of crystals and it also reveals the presence of hexagonal-shaped and rod like crystals. The average crystal size of hexagonal-shaped crystals was observed to be around 2–5 μm. Rod like crystals of 1–4 μm length were also seen.

3.3 Mechanical property evaluation of the glass ceramics

The hardness of the heat-treated glass ceramic samples is measured by acquiring micro-indentation at an indent load of 40 g and the average diagonal length of the hardness impression is calculated. For selected glass-ceramic samples, i.e., M1, M2 and M3 composition, heat treated at 1040°C for 12 h, the microhardness measurements were carried out and the hardness as well as crystal volume fractions are plotted together in Fig. 6a. The SEM image of indent impression was taken on M1 sample with 40 g load has been provided in Fig. 6b. SEM image reveals clear

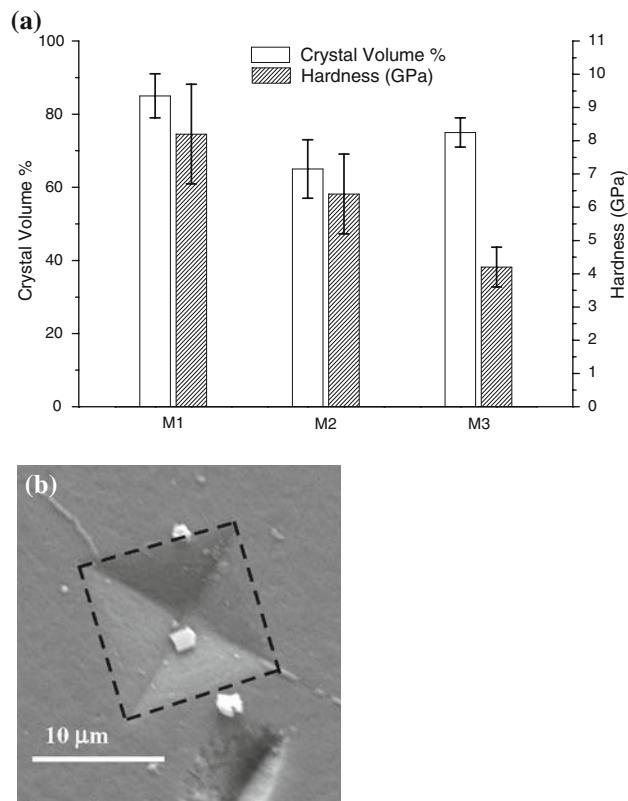


Fig. 6 **a** Plot of variation of average hardness and crystal volume fraction of M1, M2 and M3 glass-ceramics heat treated at 1040°C for 12 h. Around 20% variations in hardness value were measured and **b** SEM image of indent impression on M1 sample with 40 g load. The dotted lines in **(b)** indicate the indent edges

indent impression on the sample surface and the propagation of radial cracks from indent corners. The maximum hardness value of 8.2 GPa is found for the M1 sample. Whereas, maximum hardness values of the other two samples M2 and M3 were found to be 6.5 and 4.9 GPa, respectively. These hardness values are well above the previously reported hardness of Macor, which is not more than 2–3 GPa [16]. As expected, highest hardness is measured for GC with maximum crystal volume fraction, which is in agreement with the findings of the previous researches [30]. Other than the amount of crystal present, the aspect ratio and interlocking between the crystals also play an important role in determining the hardness. Crystals with larger aspect ratio, i.e., longer crystals are able to form an effective interlocking [30]. More amount of interlocking in the glass ceramic material actually helps in stopping the cracks more effectively, thereby enhancing the plastic deformation of the material. In the present case, M1 sample, due to the presence of highly oriented crystals with higher aspect ratio compared to the M2 and M3 samples, exhibit high hardness. For M2 and M3 samples, hardness values do not commensurate well with the crystal volume

fraction. This is because of the fact that the crystal morphology in these glass ceramics is different from M1 glass ceramic.

The basic mechanical properties, i.e., flexural strength (3-point) and E-modulus of selected samples (M1 and M2, both heat treated at 1040°C for 12 h) were measured. The experimental results reveal that a combination of relatively higher strength (94 MPa) and lower E-modulus (57 MPa) could be obtained in M1 samples. In contrast, a little lower strength of 80 GPa with better E-modulus property (69 GPa) was measured with M2 sample. The discussion on differences in mechanical properties will be made in Sect. 4.2.

3.4 In vitro property

In the present study, the in vitro dissolution of the heat-treated samples is tested in AS, in order to gain an initial knowledge about the in vitro behavior of the machinable glass ceramic materials in actual operational condition inside the oral cavity. M2 samples (heat treated at 1040°C for 12 h) were selected for in vitro dissolution test for various reasons (see Table 1 for composition). Firstly, this glass ceramic sample contains least crystal volume fraction of about 71% and lesser amount of crystal content in a glass ceramic has been reported to give better dissolution property. Secondly, its hardness value was moderate (6.4 GPa) compared to human dental enamel (4 GPa) and therefore is more suited for dental restoration purpose. The weight loss of the investigated glass-ceramic samples was measured after each dissolution test, but no weight loss or gain could be recorded within the accuracy of digital balance (three digit resolution). SEM-EDS analysis of the surface of the sample immersed in AS for different time periods of 2, 3, 6, and 8 weeks were carried out in order to assess the extent of Ca–P layer formation on the surface (Fig. 7). The observation of the SEM images in Fig. 7a reveals the formation of thin surface layers after testing for 3 weeks. With increase in further leaching time for 6 weeks, spherical particles of diameter 2–3 μm were observed to disperse densely and uniformly on the surface (Fig. 7b). EDS analysis of spherical particles indicates the strong peaks of Ca, P and O, thereby confirming the formation of Ca–P compounds. Further, the analysis of EDS data indicate that the composition of those spherical brighter contrasting particles, which cover the majority of surface area, can be characterized by Ca/P ratio of 1.57 (average). Ca–P compounds are highly bioactive and therefore, the formation of these layers on the glass ceramics sample is a good indication of the bioactive nature of the developed glass ceramic.

The leaching of F^- , K^+ , and Mg^{+2} ions, in term of absolute amount in parts per million (ppm), in the solution

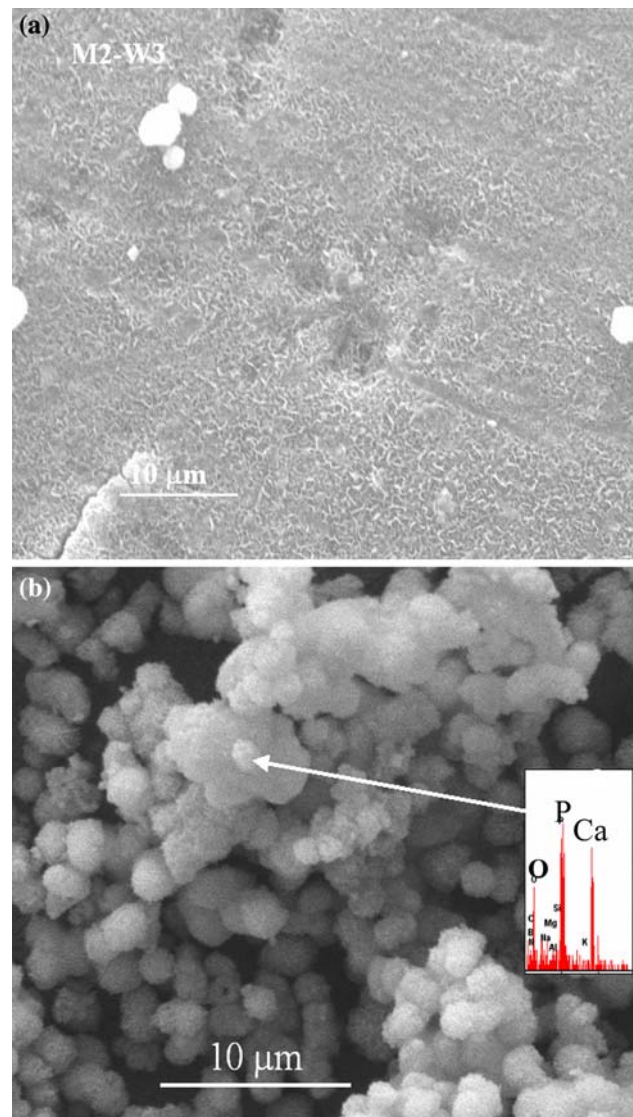


Fig. 7 SEM observation of glass-ceramic surface (M2 sample, heat treated at 1040°C for 12 h) after immersing in AS solution for **a** 3 weeks and **b** 6 weeks. EDS analysis of the brighter particles in (**b**) has been provided as inset

from the sample are plotted against time in Fig. 8a–c, respectively. The study revealed that F^- , Mg^{+2} and K^+ ions leached from the sample was 0.44, 8 and 315 ppm, respectively, after 8 weeks of immersion. The absolute amount of released F^- and K^+ ions decreased with time. Though the absolute amount of Mg^{+2} ion in the solution was increased initially, but at a later stage, it was found that the rate of leaching of Mg^{+2} ions in the solution decreases. Fig. 9 demonstrates leaching of various metal ions from the three different samples of varying composition. After 8 weeks of immersion, K^+ ions leaching from the sample surface to the AS solution has been compared for all the three samples M1, M2 and M3 (Fig. 9a). The amount of leached K^+ ions was observed maximum in M1 sample

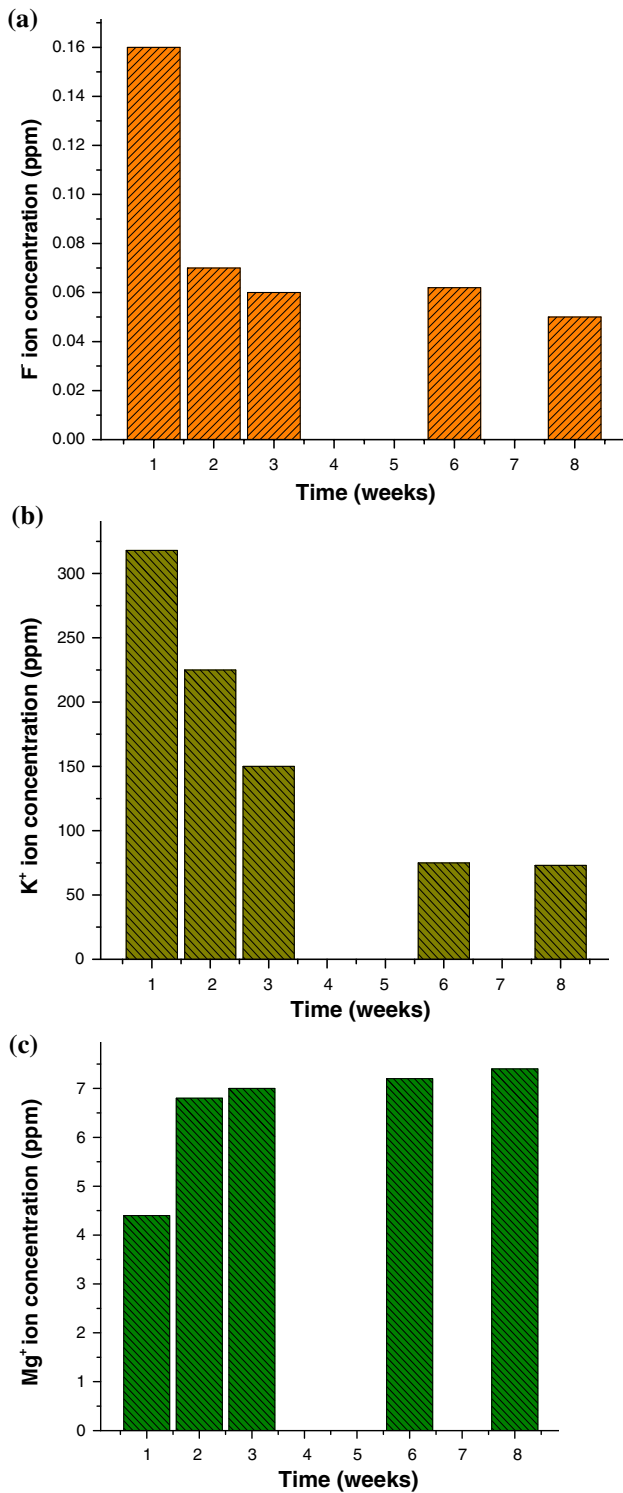


Fig. 8 Plot of absolute **a** F⁻, **b** K⁺ and **c** Mg⁺² ion concentration versus time of immersion of M2 glass-ceramic sample (heat treated at 1040°C for 12 h) in AS solution for varying time periods

(~220 ppm), compared to other two samples M2 (~75 ppm) and M3 (~80 ppm). Leaching of Mg⁺² ions in the solution was observed lower, compared to K⁺ ions leaching and followed the similar trend like K⁺ ions

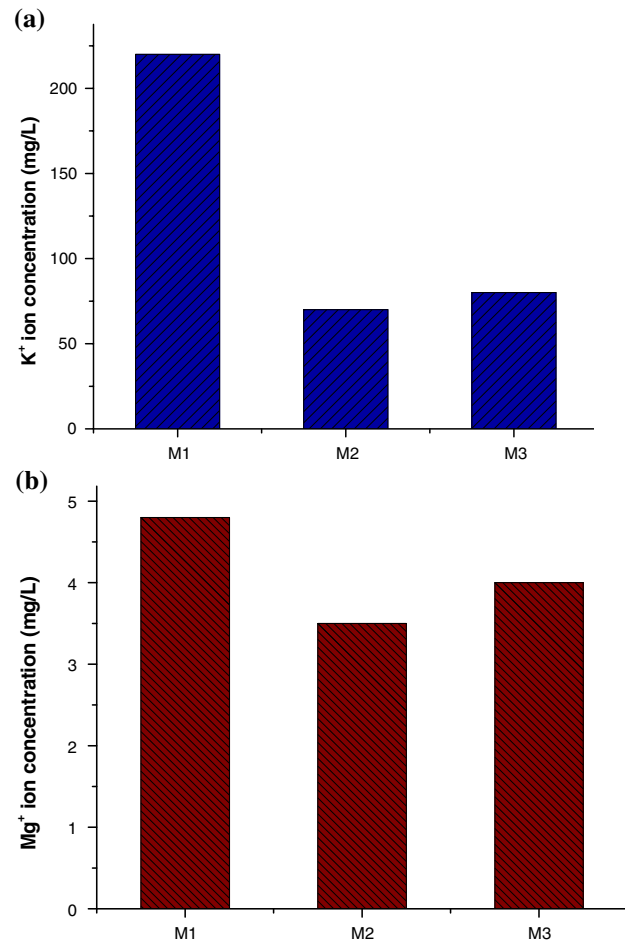


Fig. 9 **a** K⁺ and **b** Mg⁺² ion concentration in AS solution, after immersion of 8 weeks M1, M2 and M3 (heat treated 1040°C for 12 h) samples

(Fig. 9b). The leaching of Mg⁺² ions in the solution was within a range of 3.5–4.8 ppm.

4 Discussion

4.1 Microstructure development

Closer observation and comparison of XRD spectra in Fig. 1 suggest that the large diffuse and broad peak of base glass, as noticed in the 2θ range of 15–35°, has been decomposed to a number of sharp peaks with varying intensity. Such peaks were identified as FPP peaks. In addition to such observation, X-ray peak at lower $2\theta = 9^\circ$ is recorded in M1 GC compositions. Besides this, many peaks, identified for FPP phases have also been detected in the higher 2θ angle range (see Fig. 1).

The appearance of the broad and diffuse peak in DTA spectra (Fig. 2), spread over the temperature range of 700–850°C with a peak at 818°C can be correlated with two

successive events: (a) dissolution of chondrodite and (b) formation of norbergite. This explanation can be supported by earlier observations. Chyung et al. [31] also found that chondrodite phases are dissolved above 750°C and successively Norbergite phases start appearing. Again, the observation of small hump at the extended tail part, i.e., at 912°C and subsequent appearance of another peak at 1093°C could be related to the outset and consequently, complete dissolution of norbergite phase to FPP. It can be mentioned here that the nucleation temperature of FPP crystal is a strong function of heating rate, as observed by Bapna et al. [32]. It was reported that increasing heating rate shifts the occurrence of nucleation temperature to a higher value.

As far as the crystallization is concerned, highly oriented unidirectional crystals were obtained for the M1 samples, under all heat-treatment conditions. The analysis of the chemical composition of the crystallized M1 samples reveals lower content of fluorine (1.08%), as compared to other glass samples of M2 and M3. Fluorine acts as the nucleating agent in the investigated system. As the composition of the glass samples of M1, M2 and M3 is suitable for FPP crystal formation, it is expected that the phase-separated glass has grown to form FPP crystals. With reference to the sheet like structure of FPP, the composition of the system was selected in such a manner to create deficiency of cross-linking species potassium, for facilitating unidirectional growth. With less amount of nucleating species F^- and therefore, having very less number of nuclei sites in the phase-separated glass, the unidirectional growth mechanism of crystals is enhanced. A possible mechanism for this type of crystal morphology development has been shown schematically in Fig. 10. In glass ceramics based on M1 composition, the unidirectional growth of crystals can be related to the inherent crystal structure and base glass compositions.

For M2 compositions, different sizes of 5–15 μm crystals were observed on polished-etched surfaces (see Fig. 5a). The heat-treated M3 glass ceramics containing

hexagonal-shaped crystals are observed under SEM. The fluoride content of this glass-ceramic is more than M1 and slightly less than M2 samples. For this system, the availability of free space for crystal growth in all the direction leads to hexagonal-shaped crystal morphology. From the composition Table 1, it has been observed that B_2O_3 amount is highest in M3 composition. The presence of B_2O_3 enhances the mass transport by reducing the viscosity of the glass. This may be a reason for growth of crystals in all direction making the crystal hexagonal in shape.

The above observations need to be placed in the context of earlier observations, reported in literature. The “straw” like morphology of the characteristic mica crystal phase and the randomly oriented, interlocked microstructure are common and reported by previous researchers, e.g., Habelitz et al. [33], Hoche et al. [34], Ma et al. [35], Bapna et al. [32], Cripps et al. [36], and Tsuchiya et al. [37]. Some other researchers like Vogel et al. [38] and Gebhardt et al. [39] also reported a ‘Cabbage’ shaped morphology in a slightly different base glass composition (21.2 mol.% MgO, 19.5 mol.% Al_2O_3 , 59.3 mol.% SiO_2 doped with 11.2 mol.% F^- and 6.4 mol.% Na_2O/K_2O) and at a heat treatment temperature lower than 1000°C. In a recent work, Roy and Basu reported the formation of spherulitic-dendritic crystal morphology in glass ceramic system, similar to the presently investigated one [6]. In the light of the above observations, it should be clear that the variation in F^- content in base glass, in the present case, results in the development of characteristically different crystals in $K_2O-B_2O_3-Al_2O_3-SiO_2-MgO-F$ glass ceramic.

In the following, the kinetics of crystallization behavior is analyzed. The crystal volume fraction were calculated from the SEM images of all the samples using image analysis and adopting basic stereological concepts (point counting method on a grid paper superimposed on a number of SEM images), the data reveal that M1 sample heat treated at 1040°C for 12 h has the maximum average crystal volume of 85% and M2 sample heat treated at

Fig. 10 Schematic representation of formation of envelope-like crystals clearly showing crystal domain boundary analogous to grain boundary in crystals

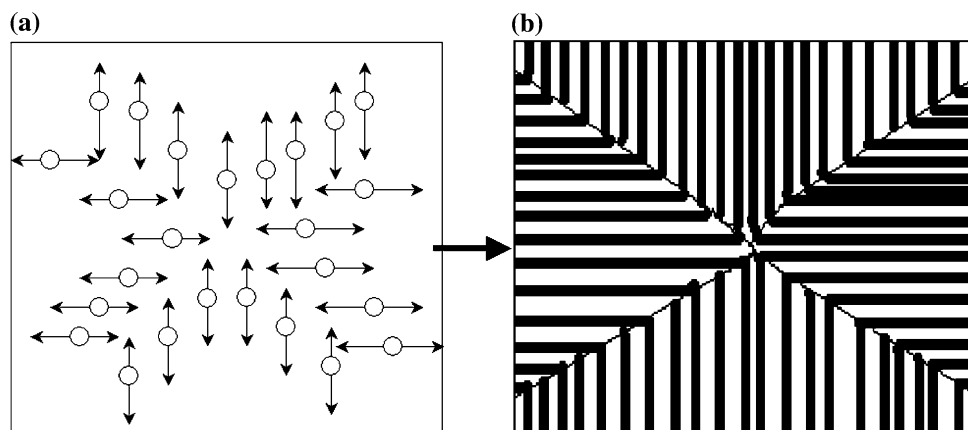


Table 3 Variation in crystalline content (measured using conventional stereology technique) obtained with different crystallization heat treatment experiments

Sample	Heat treatment condition	Crystal± volume fraction (%)
M1	1040°C, 12 h	85
	1040°C, 6 h	75
M2	1040°C, 12 h	71
	1040°C, 6 h	58
M3	1040°C, 12 h	75
	1040°C, 6 h	55

1040°C for 12 h has the average crystal content of 71% and M3 sample heat treated at 1040°C for 12 h has average 75% crystals. Most important findings from the present observation are that with an increase in fluorine content in the glass composition, the amount of crystal content decreases. The variation of crystal content with duration of crystallization time for M1, M2 and M2 sample has been provided in Table 3.

Among many theoretical models, the most widely used John–Mehl–Avrami (JMA) equation [40, 41] has been used to determine the activation energy for isothermal crystallization of mica glass ceramics:

$$-\ln(1-x) = (Kt)^n \quad (2)$$

where x is the crystallized fraction, t is the crystallization time, n is Avrami index; and K is a constant, which can be expressed by Arrhenius equation,

$$K = v \exp(-E_c/RT) \quad (3)$$

where T is the absolute temperature of crystallization, E_c is the activation energy of the crystallization and v is the frequency factor, assumed to be as $2.88 \times 10^{11} \text{ s}^{-1}$.

Based on the experimental results provided in Table 3, the Avrami index (n) was found to be 1.39 for M1 samples, 0.51 for M2 samples and 0.80 for M3 samples. It can be mentioned here that much higher value of $n = 3.4$ is reported for nucleation and crystallization of tetrasilic fluormica crystals in Dicor glass ceramics [32]. Additionally, the activation energies were found to be 272, 403, and 401 kJ/mol for M1, M2 and M3 samples, respectively. Such values are higher compared to the activation energies of Dicor glass ceramics (203 kJ/mol) [32]. Among the three samples, for M1 sample, Avrami index was maximum and also the activation energy for crystallization was lower than that of other two samples. This indicates that the rate of growth is higher than the other two samples. The activation energies for crystallization are comparable for M2 and M3 samples, despite differences in base glass composition.

4.2 Mechanical property

As mentioned in Subsect. 3.2, the evaluation of basic mechanical property reveals better hardness and strength property of M1 GC compared to that of M2 GC (see also Table 4). From the microstructure–mechanical property correlation point of view, it appears that higher volume fraction of crystalline phase and highly oriented ‘envelope’ like crystals are beneficial to obtain such better mechanical properties. However, E-modulus of M1 GC is lower than that of M2 GC. In many of the published research articles on GC, such a comprehensive measurements of all basic mechanical properties are not presented. Nevertheless, some published data on hardness or E-modulus have been collected and a comparison with mechanical properties of various other GC is made in Table 4. The properties of Dicor glass ceramics (commercially produced dental

Table 4 A comparison of mechanical property of presently investigated GC with that of earlier developed Glass ceramics/bioglass

Material	Hardness, GPa	Strength	E-modulus, GPa	Reference
Mica-apatite glass-ceramics	2.8–4.8	–	–	[35]
Macor GC	~3	–	–	[47]
SiO ₂ –Al ₂ O ₃ –MgF ₂ (MAS)	4–7	–	–	[48]
MgO–Al ₂ O ₃ –SiO ₂ –TiO ₂	9.5	–	–	[48]
Dicor	3.5	127 (biaxial)	66.9 GPa	[32]
MGC glass ceramics	–	–	49.5–70.5	[49]
Dental Enamel	3.4–4.6	–	66.2–91.1	[5]
45S5 bioglass	–	40–60 (bending)	30–50	[9]
A/W glass-ceramic	–	215 (bending)	35	[50]
KGy213 ceravital	–	–	77–88	[50]
M1	8.2 ± 1.5	94.9 ± 14.0 (3 point Flexural)	57.6 ± 2.8	Present work
M2	6.4 ± 1.2	80.6 ± 7.7 (3 point Flexural)	69.7 ± 2.9	Present work

implant material) and natural enamel has also been compared with the glass ceramics developed in the present study. From the data provided in Table 4 it is quite clear that strength and E-modulus properties obtained in our system is comparable with both the Dicor and dental enamel. However, hardness property measured in our system is much higher, i.e., almost double than that of the Dicor/enamel. From the data provided in Table 4, it should be clear that the mechanical property (flexural strength, E-modulus) measured in the present system can be compared with other glass ceramics/Bioglass. But little higher hardness of 9.5 GPa has been reported only for MgO–Al₂O₃–SiO₂–TiO₂ (MAST) system [49]. The major crystalline phases in those GC include Mg-alumino silicate, Mg-alumino titanate, etc., and in the presence of such phases in the MAST system, machinability is expected to be very poor. Other mechanical property data is not reported for MAST system. However, comparable hardness in the range of 4–7 GPa were measured by Goswami et al. [42] in magnesium aluminum silicate GC system. From the above discussion, it should be clear that the heat treatment of K₂O–B₂O₃–Al₂O₃–SiO₂–MgO–F glass ceramics composition at 1040°C for 12 h, in the present study, enables us to obtain GC with an exceptionally higher hardness of around 8.2 GPa and better combination of strength and E-modulus.

For the first time, it has been demonstrated here that how higher crystal content and envelop-like crystal morphology can attribute to the high hardness and mechanical properties in the present machinable glass ceramics system. Researchers have observed that with a high aspect ratio and crystallinity, the microhardness decreases because of high connectivity [43]. A steep decrease in the microhardness of mica GC occurs due to the connection of the mica crystals, leading to good machinability. From the microstructure of M1 sample, it is clearly visible that crystals are oriented in such a fashion that connectivity of the crystals is less. Also, the microstructure is more akin to a fiber reinforced plastic. This is believed to be the underlying cause for achieving higher hardness/strength value. Our observations also reconfirm earlier literature results that the mechanical properties of GC are not only dependent on the crystalline phase and their volume fraction, but also highly related to the spatial arrangement of the crystals [43]. In case of M3 samples, though crystal content is higher than that of the M2 sample, hardness value measured was less. From Fig. 5b, it is visible that hexagonal crystals are randomly distributed within the glassy matrix and connectivity is also higher than other two crystal morphologies (M1 and M2). SEM image also demonstrates that glassy regions are distinctly visible as isolated pockets (Fig. 5b). Due to such inhomogeneous microstructure and higher connectivity between the crystals, hardness value is comparatively less for M3 samples compared to other two samples.

4.3 In vitro property

In this sub-section, the in vitro dissolution property will be analysed critically in terms of two important aspects: (a) leaching of various metal ions and F[−] ion at different timeframe during dissolution and (b) ability of the presently investigated glass ceramics to form Ca–P rich layer in vitro.

The quantification of F[−] ion leaching in AS medium is important, because it is known that in contact with fluoride, teeth become stained due to dental fluorosis [44]. It is interesting to note that with time, for M2 glass ceramic, fluorine ion leaching decreases. The systematic decrease in F[−] concentration with time is possibly a characteristic of the time dependent, kinetic modification of the glass-ceramic surface, that occurs upon immersion in AS [45].

With increase in time of immersion of the sample in AS medium, the adherence of Ca–P layer on the surface increases, which restricts further leaching of ions from the sample surface, leading to better durability of the material. The metal ion (K⁺, Mg⁺²) leaching behavior, observed for glass-ceramic samples immersed in AS for varying time durations provide us important information. It was observed that during initial stages of the experiment, the K⁺ ions leaching were more compared to the later stages (see Fig. 8b). The systematic decrease in K⁺ ion concentration with time is characterized by a minimum amount of around 70 ppm after 6/8 weeks. In AS solution, K⁺ ions are present and K⁺ ions come in equilibrium with the leached K⁺ ions from the sample. Because of such phenomenon, K⁺ ion leaching from the solution is reduced after specific timeframe and not much difference was observed in K⁺ ion concentration in AS solution between 6 and 8 weeks of immersion.

In contrast to K⁺ ion, AS solution does not contain any Mg⁺² ion (see Table 2). The cumulative plot of Mg⁺² ion concentrations with time for glass-ceramic samples demonstrate that with increase in time, the amount of leached Mg⁺² ions increases, but rate of leaching was reduced at later stage. The increase in Mg⁺ ions from 6.5 to 7.2 ppm occurs as time of leaching increases from 2 to 8 weeks.

The AAS results plotted in Fig. 9 reveals that the amount of leached K⁺ and Mg⁺² ions is higher for M1 GC and they are comparable for M2 and M3 glass ceramic. This indicates that the leaching of metal ions from the sample surface was higher for the samples of higher crystalline content and this is in good agreement with the findings of the previous researchers [9]. This important finding ensures that with time, degradation of mechanical property of the glass-ceramic containing less crystal in AS medium will be reduced.

In summary, it can be said that the newly developed glass ceramic materials offer excellent combination of

hardness, E-modulus and strength property. It is known that the Dicor material which is being developed for dental restorative application exhibit a modest combination of hardness (350 MPa), E-modulus (66.2–91.1 GPa) and strength property (127 MPa). A comparison of presently developed material with Dicor and natural enamel is provided in Table 4. It should be understood that M1 or M2 glass ceramic can outperform Dicor. In addition, the natural human cortical bone is characterized by a combination of mechanical property, depending on anatomical location. In particular, their E-modulus is 80 GPa or less and they have tensile strength values varying in the range of 60–160 MPa [46]. Although, the tensile strength is not measured in the present case, the tensile strength of the investigated glass ceramic should be less than the measured 3-point bending strength values (94 MPa). It is therefore, apparent that the developed glass ceramic will be able to closely mimic the cortical bone properties. More importantly, the *in vitro* dissolution experiment also proves the occurrence of Ca–P layer formation for M2 GC as well as modest level of metal ion dissolution at the ppm level. The biomineralisation capability *in vitro* is expected to enhance the bone formation capability of the M2 glass ceramic *in vivo*. From the above observations, the M2 glass ceramics can be considered as a potential bone replacement material, in particular for dental restorative application. However, further investigation needs to be carried out in future to characterize the optical translucency, machinability and long-term durability property of the developed glass ceramics. Also, it will be necessary to assess the *in vitro* biocompatibility (cell viability) and *in vivo* osseointegration (clinical trials), before their applications can be realized.

5 Conclusions

The influence of various ceramising treatments on the microstructure development on three different K_2O – B_2O_3 – Al_2O_3 – SiO_2 – MgO – F base glass compositions was investigated. In particular, F^- content in base glass is varied in the range of 1.08–3.85% and a set of heat treatment experiments were carried out at 1000–1120°C for different time duration of 4–24 h. A number of characterizing techniques, including SEM-EDS, FT-IR, DTA and XRD were used and the basic mechanical properties as well as *in vitro* properties were evaluated. The important conclusions are summarized as follows:

- (a) The variation in fluorine content has a marked influence on the crystallization kinetics as well as crystal morphology. The Avrami constant is highest (~ 1.4) and the activation energy of crystallization is around 272 kJ/mol for highly oriented and characteristic ‘envelope’ like crystals in glass ceramic with 1.08% fluorine content, when heat treated at 1040°C for 12 h. Based on the DTA analysis, the glass transition (T_g) temperature is found to be around 603°C and it was revealed that the crystallization start at nearly above 750°C. In the case of glass ceramics processed from base glass with intermediate fluorine content (2.53%), a distinctly different crystal morphology, i.e., hexagonal-shaped crystals develop and the activation energy for crystallization of such morphology is found to be much higher (~ 400 kJ/mol).
- (b) Detailed analysis of the FT-IR results confirmed the presence of various Si–O–Si, Si–O and B–O stretching bonds with the characteristic absorption peaks at 1022, 697 and 1422 cm^{-1} , respectively, and Si–O–Si bending bonds at 465–509 cm^{-1} .
- (c) An important result has been that a good combination of mechanical properties with hardness of 8.2 GPa, 3-point flexural strength of 94 MPa and E-modulus of 57 GPa can be obtained in the glass ceramics with the lower F^- content (1.08%). A comparison with the existing glass ceramic materials (including Dicor, natural enamel, etc.) establishes superior mechanical properties of the newly developed glass ceramics. Higher crystal volume fraction as well as oriented ‘rod’ like crystal morphology with interlocking characteristics has been identified as the factors leading to achieving good strength/hardness.
- (d) More importantly, an adherent Ca–P rich biomineralised layer, containing spherical particles of 2–3 μm size has been found to form *in vitro* on the glass ceramics surface (3.85% fluorine), after dissolution in AS for 6 weeks. This observation indicates the biomineralisation capability of the investigated glass ceramic.
- (e) The leaching of three different ions (F^- , Mg^{+2} , K^{+1}) was measured. Fluorine ions concentration in the leached solution was about 0.15 ppm after leaching of 8 weeks, which is one order of magnitude lower than the WHO recommended maximum safety limits (1.5 ppm). Mg^{+2} and K^{+1} ions leaching were also in the ppm level and observed to decrease with dissolution time. Lower amount of metal ion dissolution is measured for glass ceramics containing higher F^- content, compared to that with glass ceramics containing 1.04% F^- .
- (f) Based on the combination of mechanical and *in vitro* properties, the glass ceramics with highest amount of F^- content (3.85%) has been proposed as a suitable material for dental restoration purpose. Also, the particular combination of E-modulus (69 GPa) and

strength (80 MPa)/hardness (6.4 GPa) property indicates that this particular grade glass ceramic can be alternatively used for hard tissue replacement/bone analogue materials. However, further clinical trials are required to confirm such potential.

References

- G.H. Beall, in *Advances in Nucleation and Crystallization in Glass*, ed. by L.L. Hench, S.W. Freiman (American Ceramic Society, Columbus, OH, 1971), Special publication no. 5, pp. 251–261
- A.R. Molla, Influence of ceramising treatment on the crystal shape, in vitro and tribological properties of machinable glass ceramics, M.Tech thesis, IIT Kanpur, India, July, 2007
- T. Uno, T. Kasuga, S. Nakayama, A.J. Ikushima, Microstructure of mica-based nanocomposite glass-ceramics. *J. Am. Ceram. Soc.* **76**(2), 539–541 (1993). Feb
- D.S. Baik, K.S. No, J.S. Chun, Mechanical properties of mica glass-ceramics. *J. Am. Ceram. Soc.* **78**(5), 1217–1222 (1995). doi:10.1111/j.1151-2916.1995.tb08472.x
- S. Roy, B. Basu, Hardness properties and microscopic investigation of crack-crystal interaction in $\text{SiO}_2\text{-MgO-Al}_2\text{O}_3\text{-K}_2\text{O-B}_2\text{O}_3\text{-F}$ glass ceramic system. *Mat. Sci. Eng. C* (provisionally accepted, 2008)
- S. Roy, B. Basu, On the development of two characteristically different crystal morphology in $\text{SiO}_2\text{-MgO-Al}_2\text{O}_3\text{-K}_2\text{O-B}_2\text{O}_3\text{-F}$ glass-ceramic system. *J. Mater. Sci. Mater. Med.* <http://dx.doi.org/10.1007/s10856-008-3536-9>, in press
- S. Roy, B. Basu, In vitro dissolution behaviour of $\text{SiO}_2\text{-MgO-Al}_2\text{O}_3\text{-K}_2\text{O-B}_2\text{O}_3\text{-F}$ glass-ceramic system. *J. Mater. Sci.: Mater. Med.* **19**, 3123–3133 (2008). doi:10.1007/s10856-008-3440-3
- S. Roy, B. Basu, Mechanical and tribological characterization of human tooth. *Mater. Charact.* **59**, 747–756 (2008). doi:10.1016/j.matchar.2007.06.008
- L.L. Hench, Bioceramics: from concept to clinic. *J. Am. Ceram. Soc.* **74**(7), 1487–1510 (1991). doi:10.1111/j.1151-2916.1991.tb07132.x
- W. Holland, W. Vogel, *An Introduction to Bioceramics* (World Scientific Publishing Company Pvt Ltd, Singapore, 1993), pp. 125–137
- W. Holland, G. Beall, *Glass Ceramic Technology* (The American Ceramic Society, Westerville, 2002)
- T. Kokubo, S. Ito, M. Shigematsu, S. Sakka, T. Yamamuro, Mechanical properties of a new type of apatite-containing glass-ceramic for prosthetic application. *J. Mater. Sci.* **20**, 2001–2004 (1985). doi:10.1007/BF01112282
- T. Kokubo, S. Ito, S. Sakka, T. Yamamuro, Formation of a high-strength bioactive glass-ceramic in the system $\text{MgO-CaO-SiO}_2\text{-P}_2\text{O}_5$. *J. Mater. Sci.* **21**, 536–540 (1986). doi:10.1007/BF01145520
- M. Akao, H. Aoki, K. Kato, Mechanical properties of sintered hydroxyapatite for prosthetic application. *J. Mater. Sci.* **16**, 809–812 (1981). doi:10.1007/BF02402799
- G. Dewith, H.J.A. Vandijk, N. Hattu, K. Prijs, Preparation, microstructure and mechanical-properties of dense polycrystalline hydroxy apatite. *J. Mater. Sci.* **16**, 1592–1598 (1981)
- D.-M. Liu, Bioactive glass-ceramic: formation, characterization and bioactivity. *Mater. Chem. Phys.* **36**, 294–303 (1994). doi:10.1016/0254-0584(94)90045-0
- P. Vincenzini (ed.), *Ceramics in Clinical Applications* (Elsevier, Amsterdam, 1987)
- T. Kitsugi, T. Yamamuro, T. Nakamura, T. Kokubo, Bone bonding behavior of $\text{MgO-CaO-SiO}_2\text{-P}_2\text{O}_5\text{-CaF}_2$ glass (mother glass of AW-glass-ceramics). *J. Biomed. Mater. Res.* **23**, 631–648 (1989). doi:10.1002/jbm.820230607
- T. Nakamuro, T. Yamamuro, S. Higashi, T. Kokubo, S. Ito, A new glass-ceramic for bone replacement: evaluation of its bonding to bone tissue. *J. Biomed. Mater. Res.* **19**, 685 (1985)
- J.B. Quinn, V. Sundar, I.K. Lloyd, Influence of microstructure and chemistry on the fracture toughness of dental ceramics. *Dent. Mater.* **19**, 603–611 (2003). doi:10.1016/S0109-5641(03)00002-2
- D.G. Grossman, Processing of dental ceramic by casting method. *Ceram. Eng. Sci. Proc.* **6**, 19–40 (1985). doi:10.1002/9780470320259.ch3
- X. Chen, L.L. Hench, D. Greenspan, Investigation on phase separation, nucleation and crystallization in bioactive glass-ceramics containing fluorophlogopite and fluorapatite. *Ceram. Int.* **24**, 401–410 (1998). doi:10.1016/S0272-8842(97)00028-X
- L. Radonjić, L. Nikolić, The effect of fluorine source and concentration on the crystallization of machinable glass-ceramics. *J. Eur. Ceram. Soc.* **7**(1), 11–16 (1991)
- K. Cheng, J. Wan, K. Liang, Crystallization of $\text{R}_2\text{O-MgO-Al}_2\text{O}_3\text{-B}_2\text{O}_3\text{-SiO}_2\text{-F}$ ($\text{R} = \text{K}^+, \text{Na}^+$) glasses with different fluorine source. *Mater. Lett.* **47**, 1–6 (2001). doi:10.1016/S0167-577X(00)00201-9
- K.J. Anusavice, N.Z. Zhang, Chemical durability of Dicor and Lithia based glass ceramics. *Dent. Mater.* **13**, 13–19 (1997)
- L.A. Flanders, J.B. Quinn, C. Otto, C. Otto, Wilson Jr., I.K. Lloyd, Scratch hardness and chipping of dental ceramics under different environments. *Dent. Mater.* **19**, 716–724 (2003). doi:10.1016/S0109-5641(03)00018-6
- H. Li, Z.R. Zhou, Wear behaviour of human teeth in dry and artificial saliva conditions. *Wear* **249**, 980–984 (2002). doi:10.1016/S0043-1648(01)00835-3
- V. Saraswati, S. Raoot, Machinable mica-based glass-ceramic. *J. Mater. Sci.* **27**, 429–432 (1992). doi:10.1007/BF00543933
- T. Furukawa, W.B. White, Raman spectroscopy of heat-treated $\text{B}_2\text{O}_3\text{-SiO}_2$ Glasses. *J. Am. Ceram. Soc.* **64**, 443 (1981). doi:10.1111/j.1151-2916.1981.tb09893.x
- M.I. Alemany, P. Velasquez, M.A. de la Casa-Lillo, P.N. De Aza, Effect of materials' processing methods on the 'in vitro' bioactivity of wollastonite glass-ceramic materials. *J. Non-Cryst. Solid* **351**, 1716–1726 (2005). doi:10.1016/j.jnoncrsol.2005.04.062
- Chyung CK, Beall GH, Grossman DG, in *10th International congress on glass*, vol 14 (reprinted by Ceramic Society of Japan, Kyoto, Japan, 1974), p. 33
- M.S. Bapna, H.J. Mueller, Study of devitrification of Dicor® glass. *Biomaterials* **17**, 2045–2052 (1996). doi:10.1016/0142-9612(96)00024-5
- S. Habelitz, T. Höche, R. Hergt, G. Carl, C. Rüssel, Microstructural design through epitaxial growth in extruded mica glass-ceramics. *Acta Mater.* **47**(9), 2831–2840 (1999). doi:10.1016/S1359-6454(99)00135-4
- T. Höche, S. Habelitz, I. Avramov, Crystal morphology engineering in $\text{SiO}_2\text{-Al}_2\text{O}_3\text{-MgO-K}_2\text{O-Na}_2\text{O-F}^-$ mica glass-ceramics. *Acta Mater.* **47**(3), 735–744 (1999). doi:10.1016/S1359-6454(98)00424-8
- X.P. Ma, G.X. Li, L. Shen, Z.H. Jin, Ductile-mode material removal of a mica-glass-ceramic. *J. Am. Ceram. Soc.* **86**(6), 1040–1042 (2003)
- A.C.F. Cripps, B.R. And Lawn, Indentation stress-strain curves for "quasi-ductile" ceramics. *Acta Mater.* **44**(2), 519–527 (1996). doi:10.1016/1359-6454(95)00204-9
- H. Tsuchiya, Y. Hoshino, K. Tajima, N. Takagi, Leaching and cytotoxicity of formaldehyde and methyl methacrylate from acrylic resin denture base materials. *J. Prosthet. Dent.* **71**(December), 619–623 (1994).

38. W. Vogel, W. Höland, K. Naumann, J. Gummel, Development of machineable bioactive glass ceramics for medical uses. *J. Non-Crystal. Solid* **80**(1–3), 34–51 (1986)
39. A. Gebhardt, T. Höche, G. Carl, I.I. Khodos, TEM study on the origin of cabbage-shaped mica crystal aggregates in machinable glass-ceramics. *Acta Mater.* **47**(17), 4427–4434 (1999). doi: [10.1016/S1359-6454\(99\)00317-1](https://doi.org/10.1016/S1359-6454(99)00317-1)
40. W.A. Johnson, R.F. Mehl, Reaction Kinetics in process of nucleation and growth. *Trans. AIME* **135**, 416–442 (1939)
41. M. Avrami, Kinetics of phase change, *J. Chem. Phys.* **7**, 1103–1112 (1939), **9**, 177–184 (1941)
42. M. Goswami, A. Sarkar, T. Mirza, V.K. Shrikhande, K.R. Sangeeta, Gurumurthy, G.P. Kothiyal, Study of some thermal and mechanical properties of magnesium aluminium silicate glass ceramic. *Ceram. Int.* **28**, 585 (2002). doi: [10.1016/S0272-8842\(02\)00013-5](https://doi.org/10.1016/S0272-8842(02)00013-5)
43. D.S. Baik, K.S. No, J.S. Chun, H.Y. Cho, Effect of the aspect ratio of mica crystals and crystallinity on the microhardness and machinability of mica glass-ceramics. *J. Mater. Process. Technol.* **67**, 50–54 (1997). doi: [10.1016/S0924-0136\(96\)02817-8](https://doi.org/10.1016/S0924-0136(96)02817-8)
44. W.B. Apambire, D.R. Boyle, F.A. Mische, Geochemistry, genesis, and health implications of fluoriferous groundwaters in the upper regions of Ghana. *Environ. Geol.* **33**(1), 13–24 (1997). doi: [10.1007/s002540050221](https://doi.org/10.1007/s002540050221)
45. L.L. Hench, R.J. Splinter, W.C. Allen, T.K. Greenlee Jr, Bonding mechanisms at the interface of ceramic prosthetic materials. *J. Biomed. Mater. Res.* **2**, 117–141 (1972)
46. B.D. Ratner, A.S. Hoffman, F.J. Schoen, J.E. Lemons, *Biomaterials Science: An Introduction to Materials in Medicine* (Academic Press, London, 2004)
47. P.S. Wuttiphan, B.R. Lawn, K. Chyung, Role of microstructure on contact damage and strength degradation of micaceous glass-ceramics. *Dent. Mater.* **14**(1), 80 (1998). doi: [10.1016/S0109-5641\(98\)00013-X](https://doi.org/10.1016/S0109-5641(98)00013-X)
48. J. Henry, R.G. Hill, The influence of lithia content on the properties of fluorphlogopite glass-ceramics. II. Microstructure hardness and machinability. *J. Non-Cryst. Solid* **319**, 13 (2003). doi: [10.1016/S0022-3093\(02\)01959-2](https://doi.org/10.1016/S0022-3093(02)01959-2)
49. T. Kasuga, M. Yoshida, T. Uno, Preparation of zirconia toughened bioactive glass-ceramics. *J Mater Sci* **23**, 2255–2258 (1988). doi: [10.1007/BF01115797](https://doi.org/10.1007/BF01115797)
50. W. Cao, L.L. Hench, *Bioact. Mater. Ceram. Int.* **22**, 493–507 (1996). doi: [10.1016/0272-8842\(95\)00126-3](https://doi.org/10.1016/0272-8842(95)00126-3)